

ARTICLES

A common mass scaling for satellite systems of gaseous planets

Robin M. Canup¹ & William R. Ward¹

The Solar System's outer planets that contain hydrogen gas all host systems of multiple moons, which notably each contain a similar fraction of their respective planet's mass ($\sim 10^{-4}$). This mass fraction is two to three orders of magnitude smaller than that of the largest satellites of the solid planets (such as the Earth's Moon), and its common value for gas planets has been puzzling. Here we model satellite growth and loss as a forming giant planet accumulates gas and rock-ice solids from solar orbit. We find that the mass fraction of its satellite system is regulated to $\sim 10^{-4}$ by a balance of two competing processes: the supply of inflowing material to the satellites, and satellite loss through orbital decay driven by the gas. We show that the overall properties of the satellite systems of Jupiter, Saturn and Uranus arise naturally, and suggest that similar processes could limit the largest moons of extrasolar Jupiter-mass planets to Moon-to-Mars size.

Orbiting Jupiter, Saturn and Uranus are the so-called regular satellites—which orbit approximately within the planet's equatorial plane, in the same sense as the planet's rotation, and at orbital distances of up to tens of planetary radii—and much smaller irregular satellites, with more distant, inclined and elliptical orbits. Whereas irregular satellites are thought to be captured objects¹, regular satellites are believed to have arisen as a by-product of the planet's formation, within a circumplanetary disk of gas and solids^{2–4}. Outer planet satellite origin is important both for the history of these objects (including volcanic Io, Europa with its believed subsurface ocean, and organic-rich Titan) and because their existence holds clues to giant planet origins.

The number and individual masses of large satellites differ from planet to planet (Table 1). However, the systems share a distinctive trait: they each contain a similar total mass, M_T , compared to that of their central planet, M_P , with (M_T/M_P) varying only from 1.1×10^{-4} to 2.5×10^{-4} . This similarity is remarkable, and its cause unknown. The bulk compositions of the gas planets differ, and as such their satellite system masses are not a common fraction of each planet's solid (rock+ice) or gaseous (H+He) components. Additionally, $(M_T/M_P) \approx 10^{-4}$ is orders of magnitude smaller than the mass ratios of the large satellites of solid planets, with the Moon and Pluto's moon, Charon, having $(M_T/M_P) = 0.012$ and ~ 0.1 , respectively. Neither Jupiter nor Saturn, for instance, has such a proportionally massive Earth-sized satellite.

Gas planet satellite formation models have historically used as their initial condition a circumplanetary disk containing a total mass in gas and solids necessary to produce the satellites we see. Such an initial condition is, by definition, *ad hoc*, given both the rapid evolution of circumplanetary material compared to planetary formation timescales and dynamical processes that can cause much of the material supplied to such a disk to be eventually collected by the planet. Thus a planet's current satellites may provide little constraint on the total mass that was processed through its disk.

Here we consider a model in which satellites grow within an actively supplied circumplanetary disk, sustained by a time-dependent inflow of gas and solids from heliocentric orbit during the end stages of the planet's formation. We use both numerical

simulation and analytical estimates to describe the supply of material to the disk, satellite growth, and satellite orbital decay and loss caused by satellite interactions with the gas. We find that a common satellite system mass fraction of $\sim 10^{-4}$ results, independent of the total mass processed through the disk and only weakly dependent on the least certain model parameters. We also for the first time generate satellite systems with properties generally consistent with those of Jupiter, Saturn and Uranus using direct simulation.

Slow-inflow disk model

During a jovian planet's early growth, its massive gaseous atmosphere is distended to $\sim 10^2$ to 10^3 times the current sizes of Jupiter or Saturn⁵. The final stages of its growth involve both a slowing in the rate of gas inflow to the planet (for example, as the local supply of material is depleted or the circumsolar gas nebula begins to dissipate⁵), and the planet's gravitational contraction, which is accompanied by the formation of a circumplanetary disk^{6–8}. We model satellite growth within such a disk⁹, supplied by an inflow of gas and solids to circumplanetary orbit across a region extending roughly from the planet's surface to an outer distance of a few tens of planetary radii (Fig. 1). The disk gas diffuses viscously, causing it to radially spread. For a gas spreading time short compared to the characteristic time over which the inflow changes, the amount of gas in the disk can be estimated as a quasi-steady state between the inflow supply and removal as gas spreads inwards onto the planet and outwards to the disk's outer edge. Solids smaller than metre-scale are bound aerodynamically to the gas, and are delivered with it from heliocentric orbit to the disk. Once in circumplanetary orbit, rapid mutual collisions allow particles to grow large enough to decouple from the gas before they can be removed by aerodynamic drag⁹. Continued satellite growth then occurs with an overall rate controlled by the rate of solid inflow⁹.

Satellite growth and loss

A satellite's orbit is affected by torques resulting from its gravitational interactions with the gas. The satellite's gravity induces spiral density waves in the gas disk, and the interaction of these waves with the satellite yields a net negative torque that acts as a drag on the satellite's

¹Space Studies Department, Southwest Research Institute, Boulder, Colorado 80302, USA.

Table 1 | Regular satellite systems

Planet	Per cent high-Z mass	M_T/M_P	Number with $m_S/M_P > 10^{-8}$	Number with $m_S/M_P > 10^{-5}$	a_{\max}/R_P of most distant with $m_S/M_P > 10^{-8}$	$\langle C_{lg} \rangle$ (R_H)
Jupiter	~3–12% ⁴¹	2.1×10^{-4}	4	4	26	15.1
Saturn	~12–30% ⁴¹	2.5×10^{-4}	7	1	59	18.4
Uranus	~75–90% ³	1.1×10^{-4}	5	4	23	14.5

Shown (left to right columns) are the planet, the planet's estimated mass fraction of high-Z elements (rock + ice), total satellite system mass (M_T) scaled to the planet mass (M_P), number of satellites having individual masses $m_S > 10^{-8}M_P$, number of large satellites having $m_S/M_P > 10^{-5}$, semi-major axis in planetary radii (a_{\max}/R_P) of the most distant satellite having $m_S/M_P > 10^{-8}$, and the average large satellite orbital spacing in mutual Hill radii, $\langle C_{lg} \rangle$, with $\langle C_{lg} \rangle$ for Saturn calculated for the Rhea-to-Titan spacing. The mutual Hill radius of two satellites of masses m_1 and m_2 and orbital radii a_1 and a_2 is $R_H = 0.5(a_1 + a_2)[(m_1 + m_2)/(3M_P)]^{1/3}$, with $\Delta a = (a_2 - a_1) = CR_H$. Jupiter's four similarly sized satellites each contain within a factor of about two of the Moon's mass, with Io and Europa (having $a/R_P = 5.9$ and 9.4 , respectively) being rock-dominated, while Ganymede and Callisto (with $a/R_P = 15$ and 26.3) are a mixture of roughly half rock, half ice. We have proposed⁹ that these four satellites formed during the waning stages of inflow to Jupiter (with $\tau_G > 5 \times 10^6$ yr), and identified disk conditions consistent with the satellites' compositions, their survival against orbital decay, and a prolonged formation time required for Callisto's apparent state of incomplete differentiation^{2,42}. Saturn's system is dominated by Titan at (a/R_P) = 20.3, which contains ~96% of the total saturnian satellite system mass and is composed of about half rock, half ice. Between $3 < a/R_P < 9$ at Saturn are much smaller satellites containing a few per cent of Titan's mass, and having a variety of compositions, ranging from mixtures of rock and ice to nearly all ice⁴³. The uranian system is similar to that of Jupiter's in structure, but all four of its large satellites have densities implying roughly half-rock, half-ice compositions.

orbit. The torque is proportional to $(m_S/M_P)^2$, where m_S is the satellite's mass, while the satellite's orbital angular momentum is proportional to (m_S/M_P) . Thus density wave torques become more important as satellites grow.

Interactions with density waves circularize satellite orbits^{10–12}, and on a longer timescale, cause their orbital radii to decay through so-called type I migration^{13,14}. The associated eccentricity (e) and semi-major axis (a) decay timescales, $\tau_e = e/|\dot{e}|$ and $\tau_1 = a/|\dot{a}|$, are given by:

$$\tau_1 = \frac{1}{C_a \Omega} \left(\frac{M_P}{m_S} \right) \left(\frac{M_P}{r^2 \sigma_G} \right) \left(\frac{H}{r} \right)^2 = \frac{C_e}{C_a} \frac{\tau_e}{(H/r)^2} \quad (1)$$

where C_a and C_e are constants of order unity^{15,16}, σ_G is the disk gas surface density, $\Omega = (GM_P/r^3)^{1/2}$ is the keplerian angular velocity at radius r , and H is the vertical thickness of the gas with sound speed c , with $(H/r) \approx (c/r\Omega) \approx 0.1$.

In a disk supplied by an ongoing inflow, a satellite grows until it reaches a critical mass for which the characteristic time for its further growth is comparable to its type I orbital decay timescale. Satellites

cannot grow substantially larger than this critical mass before they are lost to collision with the planet. The accretion timescale for a mass m_S satellite is $\tau_{\text{acc}} \approx fm_S/(2\pi r \Delta r F_{\text{in}})$, where F_{in} is the inflow flux per area, f is the gas-to-solids mass ratio in the inflow, and $2\pi r \Delta r$ is the annular disk area over which the satellite accumulates material. We find (see Supplementary Notes) that the annulus width is a function of a satellite's characteristic maximum eccentricity, e , with $\Delta r/r \approx 2e$ and $e \approx (H/r)(m_S/4\pi r H \sigma_G)^{1/5}$, owing to a balance between eccentricity damping by density waves and excitation via gravitational scatterings with similarly sized objects¹⁷. Using such an estimate for Δr gives $\tau_{\text{acc}} \approx (f \sigma_G / F_{\text{in}})(m_S/4\pi r H \sigma_G)^{4/5}$.

The critical maximum satellite mass, m_{crit} , is then found by setting $\tau_{\text{acc}} = \tau_1$ from equation (1) and solving for $m_S = m_{\text{crit}}$. In quasi-steady state, the gas surface density σ_G is proportional to the inflow rate and inversely proportional to the rate at which the gas disk spreads, with the latter parameterized by a dimensionless constant¹⁸ α (so that $\sigma_G \propto (F_{\text{in}}/\alpha)$; see also Fig. 1 legend). We simplify by considering a uniform inflow flux per area across the disk interior to a radius r_C , so that $F_{\text{in}} \approx M_P/(\pi r_C^2 \tau_G)$, where $\tau_G \equiv M_P/(dM/dt)^{-1}$ is

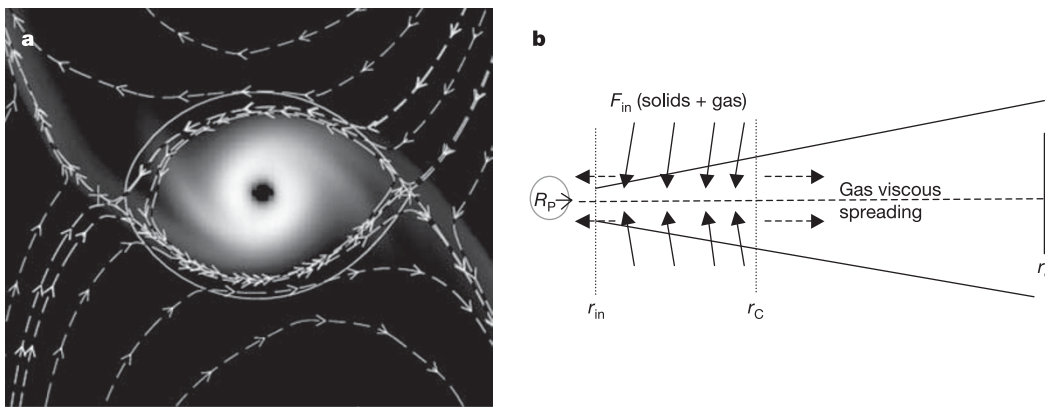


Figure 1 | An inflow-supplied circumplanetary disk. **a**, Hydrodynamical model⁶ of gas inflow into the Hill sphere (solid line) of a jovian-mass planet, viewed from above. Brightness scales with gas density; flow streamlines are dashed. **b**, The disk model considered here⁹, viewed edge-on. Gas and small solids from heliocentric orbits flow into the disk (indicated by solid arrows) across a region extending from an inner radius r_{in} to an outer radius, r_C , with an inflow flux per area $F_{\text{in}} \propto (1/r)^{\gamma_{\text{in}}}$ (where r is orbital radius and γ_{in} is an input parameter), with F_{in} containing a mass ratio f of gas-to-solids. Once in orbit, the gas viscously spreads (indicated by dashed arrows) with timescale $\tau_v \approx r^2/\nu$ and a viscosity¹⁸ $\nu = \alpha c H$, where $\alpha < 1$ is a parameter characterizing the strength of viscous turbulence in a gas disk of sound speed c and vertical state height H . When $\tau_v \ll F_{\text{in}}/F_{\text{in}} \equiv \tau_{\text{in}}$, the gas maintains a quasi-steady-state surface density, σ_G (ref. 9). For $\gamma_{\text{in}} = 0$ and $r \leq r_C$, $\sigma_G \approx (0.3 F_{\text{in}} r_C^2 / \nu) [1.2 - \sqrt{r_C/r_d} - (r/r_C)^2/4] \approx 0.2(1/\alpha) \times (F_{\text{in}} \Omega^{-1})(r/H)^2(r_C/r)^2$, with the bracketed quantity estimated for

$(r/r_C) = 0.5$ and $(r_C/r_d) = 0.2$ (ref. 9), where r_d is the disk outer edge and Ω is orbital frequency at radius r . Analytical estimates (see text) suggest that r_C is on the order of a few times $10R_P$, although because the planet's gravity alters the gas density and flow in its vicinity, hydrodynamical simulations are needed for improved estimates. Protostellar disk models⁵ consider $10^{-4} < \alpha < 0.1$, and $\tau_v \approx (1/\alpha)$ yr for protosatellite disks with $r \approx r_C \approx 30R_P$. While the source of viscosity in un-ionized disks is debated, several processes could contribute to protosatellite disks, including turbulence due to the velocity differential between inflowing and orbiting gas⁴⁴, baryonic instability⁴⁵, and density wave torques from the satellites^{9,46}. Solar composition material has $f \approx 10^2$, while the bulk compositions of Jupiter and Saturn are in the range $f \approx 3$ to 30 (Table 1). During the satellite formation era, f could have been larger than solar if most solids were contained in large objects, or smaller if some of the gas nebula had already dissipated and fragmentation had maintained a supply of small material.

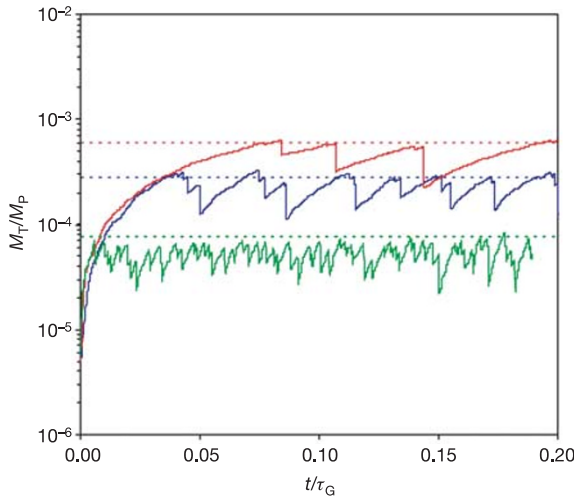


Figure 2 | Results of satellite accretion simulations with time-constant inflows. The total mass in satellites, M_T , scaled to the planet's mass, M_P , is shown versus time scaled to $\tau_G \equiv M_P / (dM/dt)^{-1}$, where dM/dt is the inflow rate. All three cases consider inflows having $\tau_G = 5 \times 10^6$ yr, $r_C = 30R_P$, and $\gamma_{in} = 0$, with the green, blue and red lines corresponding respectively to simulations with $(\alpha/f) = 10^{-6}$, 5×10^{-5} and 5×10^{-4} . The inflow of solids causes M_T to increase with time until objects of mass $\sim m_{crit}$ form (equation (2)). The orbits of the largest satellites then decay inward, and M_T decreases in discrete steps as satellites are lost to collision with the planet. Solid inflow to the disk continues, leading to the growth of another generation of mass $\sim m_{crit}$ objects, and the cycle repeats. As (M_T/M_P) depends on $(\alpha/f)^{1/3}$, the factor of 500 variation in (α/f) across these simulations yields about a factor of 10 spread in the characteristic system mass fractions. The long period oscillations in (M_T/M_P) reflect the time needed to deliver mass sufficient to form mass m_{crit} objects; this period shortens as (α/f) (and therefore (m_{crit}/M_P)) is decreased for a fixed τ_G . Shorter period variations result from the loss of individual objects. Dashed lines are predicted (M_T/M_P) values (equation (3)). Equations (2) and (3) treat disk annuli independently but in actuality, as satellites formed in the outer disk migrate inwards they pass through interior zones and cannibalize material along the way. Migration-driven growth hastens their orbital decay, so that they are lost somewhat more quickly than the time needed to replenish their mass in their original radial zone. This causes both a spread in the maximum satellite mass at a given time compared to equation (2), and the (M_T/M_P) value from equation (3) to be an approximate upper limit, as seen here.

the timescale for delivery of mass M_P . The critical satellite mass in planet masses is then (see also Supplementary Notes):

$$\begin{aligned} \left(\frac{m_{crit}}{M_P}\right) &\approx 5.4 \left(\frac{\pi}{C_a}\right)^{5/9} \left(\frac{H}{r}\right)^{26/9} \left(\frac{r}{r_C}\right)^{10/9} \left(\frac{\alpha}{f}\right)^{2/3} (\Omega\tau_G f)^{1/9} \\ &\approx 5.6 \times 10^{-5} \chi \left(\frac{3.5}{C_a}\right)^{5/9} \left(\frac{H/r}{0.1}\right)^{26/9} \left(\frac{r/r_C}{0.5}\right)^{10/9} \left(\frac{\alpha/f}{3 \times 10^{-5}}\right)^{2/3} \end{aligned} \quad (2)$$

where $\chi \equiv [(1 \text{ week}/\{2\pi/\Omega\})(f/10^2)(\tau_G/10^7 \text{ yr})]^{1/9}$ is of order unity. The ratio (m_{crit}/M_P) depends extremely weakly on the inflow rate through the $(\tau_G)^{1/9}$ term in χ . Thus a similar maximum satellite mass would result for a wide range of inflow rates. The disk aspect ratio, (H/r) , is a slowly varying quantity with r for most disks, with $(H/r) \approx 0.1$ (ref. 9). Although r_C could potentially vary substantially between planets, so long as satellites form throughout the inflow region, the ratio (r/r_C) will be similar and of order unity for the largest satellites. The last term in equation (2) contains the ratio of two key parameters: the viscosity α parameter, and the gas-to-solids ratio in the inflow, f . For a given inflow flux, a higher viscosity yields lower disk gas surface densities, and thus allows larger mass satellites to survive against type I decay, while a lower f implies a more solid-rich inflow, which hastens the rate of satellite growth so that objects grow larger before they are lost.

We now consider the implications of this limiting mass for the total mass of the resulting satellite system. Consider an inflow that persists for a time exceeding that needed for a satellite of mass m_{crit} to form. Within a given annulus in the disk, a satellite grows to a mass $\sim m_{crit}$ before being lost to type I decay, but in a comparable timescale to its loss another similarly massive satellite grows in its place (because $\tau_1 \approx \tau_{acc}$). In this way, the disk is regulated to contain a total mass in satellites, M_T , comparable to a distribution of mass m_{crit} objects across the inflow region. For (H/r) and f that are approximately constant across the disk, the predicted satellite system mass fraction is:

$$\begin{aligned} \left(\frac{M_T}{M_P}\right) &= \int_{R_P}^{r_C} \frac{(m_{crit}/M_P)}{\Delta r} dr \\ &\approx 3.5 \left(\frac{1}{C_a}\right)^{4/9} \left(\frac{H}{r}\right)^{10/9} \left(\frac{\alpha}{f}\right)^{1/3} \frac{1}{(\Omega\tau_G f)^{1/9}} \\ &\approx 2.5 \times 10^{-4} \frac{1}{\chi} \left(\frac{3.5}{C_a}\right)^{4/9} \left(\frac{H/r}{0.1}\right)^{10/9} \left(\frac{\alpha/f}{3 \times 10^{-5}}\right)^{1/3} \end{aligned} \quad (3)$$

similar to the observed satellite systems. Here we assume $r_C \gg R_P$, where R_P is the planet's radius. Note that (M_T/M_P) is insensitive to inflow rate through χ , lacks a dependence on r_C , and depends quite weakly on (α/f) .

Simulation results

We model satellite growth and loss using a direct N -body accretion simulation¹⁹, modified to include interactions with a gas disk and ongoing mass inflow (Supplementary Methods). The solid inflow is mimicked by the addition of orbiting objects with random positions within the inflow region at a rate proportional to (F_{in}/f) . Collisions are treated as inelastic mergers.

Figure 2 shows results of three simulations involving a time-constant gas inflow rate but varied values for (α/f) . Type I orbital decay acts as a negative feedback on the total mass contained in the satellite system, causing (M_T/M_P) to oscillate about a value comparable to the equation (3) estimate. Figures 3 and 4 show results of exponentially decaying, time-dependent inflows. If the total mass in solids delivered to the disk is comparable or greater than M_T , one or more satellite systems described by equations (2) and (3) result. For example, a solar composition ($f \approx 10^2$) inflow that provided the last 10% of a planet's mass could yield approximately five satellite systems with $M_T/M_P = 2 \times 10^{-4}$.

Comparison with observed satellite systems

Our findings reveal a range of systems, within which the most basic properties of the jovian, saturnian and uranian satellite distributions are found (Fig. 3; Supplementary Figures). These three planets' varied masses and compositions imply that they would have probably processed very different amounts of material through their proto-satellite disks, and yet their satellite system mass ratios are nearly identical. The results here predict this commonality, as the balance between inflow-regulated satellite growth and gas-driven satellite loss causes the total satellite mass fraction to maintain a roughly constant value, which is nearly independent of both the inflow rate and its characteristic specific angular momentum (which, as shown below, determines r_C). Thus, for example, a Jupiter-like gas giant which acquired most of its mass through gas inflow from a strongly perturbed disk (Fig. 1a) is predicted to share a common satellite mass fraction with that of a much smaller uranian-sized planet, whose gas inflow history and gravitational effects on the local nebula would have been substantially different. This common fractional value is determined primarily by the ratio of two parameters describing the disk's viscosity (α) and the inflow's gas-to-solid composition (f). A weak dependence on this ratio, with $(M_T/M_P) \propto (\alpha/f)^{1/3}$, implies that satellite system masses similar to those of

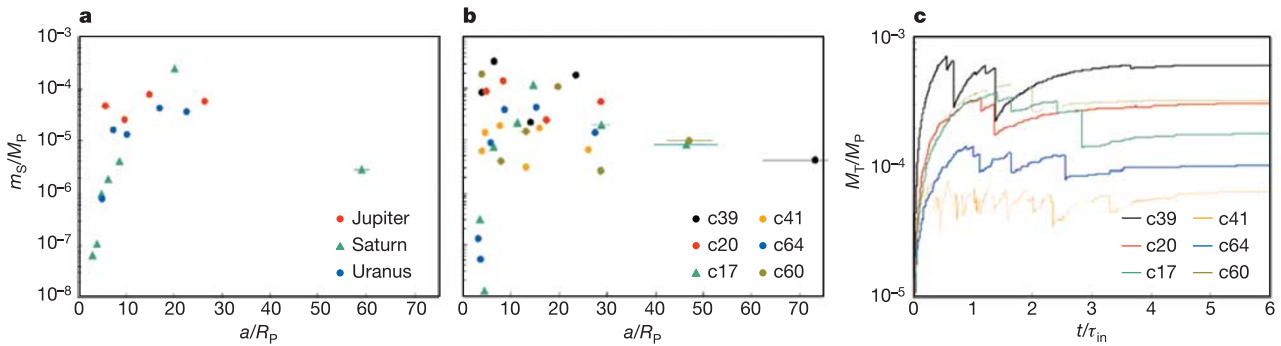


Figure 3 | Properties of observed satellites compared to simulations. Panel **a** shows observed satellites, while panels **b** and **c** contain final simulated systems produced by time-dependent inflows (with m_s , satellite mass; M_p planetary mass). Panels **b** and **c** show results of inflows with $\gamma_{in} = 0$, $r_C = 30R_p$, $1.7 < M_{in}/M_T < 10$ (where M_{in} is the total mass in solids delivered to the disk), and inflow exponential decay times, τ_{in} , between 2×10^5 yr and 1.5×10^6 yr. Systems were simulated for between 3×10^6 yr and 10^7 yr. Similar results are expected for higher M_{in}/M_T values (corresponding to longer decay times and/or higher initial inflow rates), provided that the corresponding inflow rate is consistent with a contracted planet and a circumplanetary disk. Horizontal lines connect periapse to apoapse for each satellite. **b**, A high, $(\alpha/f) = 5 \times 10^{-4}$ case, with $\alpha = 0.05$, produces five satellites with $(M_T/M_p) = 6.1 \times 10^{-4}$ (c39, black), while a low,

$(\alpha/f) = 10^{-6}$ case, with $\alpha = 10^{-4}$, produces six satellites containing $(M_T/M_p) = 6.6 \times 10^{-5}$ (c41, yellow). An $(\alpha/f) = 6.5 \times 10^{-5}$ case with $\alpha = 0.0065$ produces a galilean-like system with $(M_T/M_p) = 3.0 \times 10^{-4}$ (c20, red), while an $(\alpha/f) = 1.3 \times 10^{-5}$ case with $\alpha = 0.0065$ produces a uranian-like system with $(M_T/M_p) = 10^{-4}$ (c64, blue). A saturnian-like system with $(M_T/M_p) = 1.8 \times 10^{-4}$ (c17, green) results for $(\alpha/f) = 6 \times 10^{-5}$ and $\alpha = 0.006$. The most massive satellite at $14.6R_p$ contains $1.2 \times 10^{-4} M_p$ and 70% of the total satellite system mass, and its close orbital spacing to the satellite at $11.3R_p$ (with $C \approx 7$ in mutual Hill radii) suggests a future collision may occur²⁰ (Supplementary Notes). An $(\alpha/f) = 1.2 \times 10^{-4}$ case (c60, olive) yields $(M_T/M_p) = 3.3 \times 10^{-4}$, and two large satellites containing $0.9M_T$, with the innermost having nearly been lost to inward decay. **c**, (M_T/M_p) versus scaled time for the simulations shown in **b**.

Jupiter, Saturn and Uranus result for $10^{-6} < (\alpha/f) < 5 \times 10^{-4}$, that is, a span of nearly three orders of magnitude. Although reliable predictions for α and f are lacking, commonly used values (Fig. 1 legend) fall throughout this range.

The jovian and uranian systems each have four similarly sized large satellites, while Saturn has a single large satellite and numerous smaller satellites. Both morphologies can result from cycles of satellite formation and loss, depending on the timing of inflow cessation relative to the mass fraction oscillations seen in Fig. 2. As a system containing multiple, similarly sized satellites (for example, run c20 in Fig. 3b) undergoes orbital decay, it evolves through

periods in which only one or two of the largest satellites remain (for example, runs c17 and c60 in Fig. 3b), accompanied by much smaller moons that have accumulated in the regions vacated by the lost satellites, with this cycle repeating until the inflow ceases.

The median number of final satellites in our 75 simulated systems was $N = 7$. Future collisions on timescales longer than those simulated here are possible in many cases²⁰ (Supplementary Notes), which would generally reduce N . As our added objects are larger than those physically expected due to the inflow, the smallest final satellites resulting from only a few mergers were not well resolved. The median number of large satellites with $(m_s/M_p) \geq 10^{-5}$ was $N_{lg} = 4$. These objects had average orbital separations $\langle C_{lg} \rangle \approx 17$ comparable to both those of the outer planets (see Table 1) and our analytic estimates (Supplementary Notes).

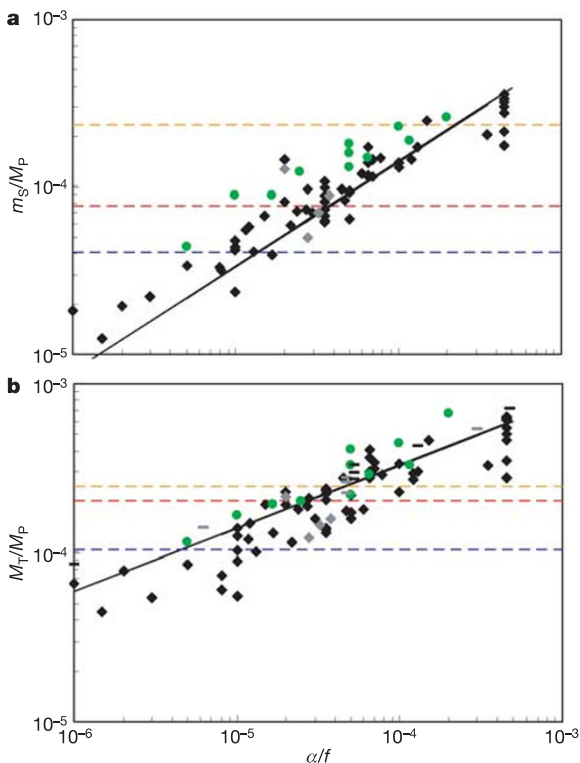


Figure 4 | Results of accretion simulations with time-dependent inflows. We consider $F_{in}(t) = F_{in}(0) \exp(-t/\tau_{in})$ and $\sigma_G(t) = \sigma_G(0) \exp(-t/\tau_{in})$, where τ_{in} is the inflow decay time (with $10^5 \leq \tau_{in}$ (years) $\leq 2 \times 10^6$) and $t = 0$ is when we begin to follow the system's evolution. Grey, black and green symbols correspond to cases with $(r_C/R_p) = 25, 30$ and 44 , respectively, while the red, orange and blue dashed lines show observed values for Jupiter, Saturn and Uranus. **a**, Maximum final satellite mass scaled to M_p versus (α/f) . (α , viscosity parameter; f , gas-to-solids ratio in the inflow.) **b**, Final satellite system total mass scaled to M_p versus (α/f) . Individual dashes are peak values from simulations with time-constant inflows (for example, Fig. 2). In **a** and **b**, black lines are equations (2) and (3) with $(r/r_C) = 0.5$, $(c/r\Omega) = 0.1$, $\tau_{in} = 10^6$ yr, and $\tau_G = \tau_{G,last} \approx \tau_{in}(M_p/M_T)/f$, corresponding to the last generation of satellites. The viscosity α values were estimated⁹ using an effective planet temperature $T_p = 500$ K and disk opacity $K = 0.1$; smaller (larger) values would result if T_p and/or K were higher (lower). By considering type I migration, we assume satellites do not grow massive enough to open annular gaps in the gas, at which point they transition to type II behaviour and are typically locked to the disk's viscous evolution^{14,47}. An estimate of the gap opening mass is⁴⁸ $m_{Gap}/M_p \approx C_v \sqrt{\alpha} (H/r)^{5/2}$, where C_v is a constant $\sim 1-10$. Our largest final satellites are all less massive than m_{Gap} for $C_v = 3$, with an average $\langle m_{lgst}/m_{Gap} \rangle = 0.2 \pm 0.1$. In an inflow-supplied disk, satellites are generally lost to type I decay before they grow to m_{Gap} . Type II behaviour would tend to accelerate orbital decay relative to type I (because $\tau_v \ll \tau_1$ for disks here), accentuating the limiting effects on M_T and m_s that we emphasize.

We find systems with maximum satellite orbital radii similar to those observed ($20 < a_{\max}/R_p < 60$) for an inflow outer radius (r_C) between 25 and 44 planetary radii (R_p), with up to a factor of two variation in a_{\max} for fixed r_C owing to scattering and migration (Supplementary Fig. 2). This range for r_C is comparable to that implied by a three-dimensional estimate^{21,22} of the net specific angular momentum, j , of uniform density material entering a sphere of radius R_H (see below), neglecting the planet's gravity. This gives $j = \Omega_p R_H^2/5$ (where Ω_p is the planet's heliocentric orbital frequency, $R_H = a_p(M_p/3M_\star)^{1/3}$ is its Hill radius, a_p its semi-major axis, and M_\star is the Sun's mass), implying a characteristic circumplanetary orbital radius $r_\star = j^2/GM_p$, with $r_\star/R_p \approx 10$ to 35 for Jupiter, Saturn and Uranus. A uniform inflow flux per area within r_C has $\langle j \rangle = \sqrt{GM_p r_\star}$ when $r_C \approx 1.6r_\star$.

Satellite compositions constrain the inflow properties during their growth, as the disk's effective temperature is a function of inflow rate (with $T_{\text{eff}} \propto F_{\text{in}}^{1/4}$, ref. 9). Thus early satellites forming during faster inflows (with smaller τ_C) would have masses set by equations (2) and (3) but rock-rich compositions (and a somewhat larger f)^{9,23}. As inflow slows, ice is increasingly incorporated. As an example, a final generation of jovian satellites produced by a solar composition inflow with a $\tau_{\text{in}} = 10^6$ -yr decay timescale (comparable to solar nebular lifetimes²³) would form within a disk having temperatures below 200 K exterior to about $15R_p$ (with α approximately equal to a few $\times 10^{-3}$, a disk opacity²⁴ $K = O(10^{-1})\text{cm}^2\text{g}^{-1}$, and a planet temperature $T_p \approx 500$ K, ref. 9), consistent with Jupiter's outer icy moons. For a planet with a much lower mass and temperature³, a mixture of ice and rock consistent with the uranian satellite compositions is expected throughout most of the disk.

In our most Saturn-like systems (for example, c17 in Fig. 3b and Supplementary Fig. 1), one or more inner companions to the final 'Titan' collided with the planet. When an inner large satellite is lost as the inflow wanes, satellites containing a much smaller total mass that form in its place derive their material from cooler disk conditions than those which predominated during earlier growth. For a solar composition inflow with $\tau_{\text{in}} = 10^6$ yr, the last 10% of a satellite system with $(M_T/M_p) \approx O(10^{-4})$ is delivered at rates slow enough that the ice stability line moves inward to a few planetary radii for a Saturn-like planet. This would allow for ice incorporation in Saturn's small inner satellites.

Whereas our results offer strong support for a common mode of origin for the satellites of gas giants (like Jupiter and Saturn), the uranian system remains more uncertain. The uranian satellites' properties are consistent with those produced here, but the 98° tilt of Uranus' rotational axis requires additional explanation. A giant impact could have been responsible²⁵, with the current satellites forming subsequently. It is not obvious that post-impact gas inflow could yield retrograde satellites (that is, regular satellites of a retrograde spinning Uranus), although retrograde circumplanetary disks have resulted in some simulations of gas inflow to approximately Uranus-sized planets²⁶. The substantial $\sim 27^\circ$ obliquity of Saturn probably resulted from spin-orbit resonant interactions^{27,28}, which caused the planet's obliquity to change slowly enough that pre-existing regular satellites would have tracked its shift and remained aligned with the planet's equatorial plane²⁹. Recent work argues for a similarly gradual origin of Uranus' obliquity³⁰. Our results reveal an advantage in linking the uranian satellites to formation from an inflow-supplied rather than an impact-produced disk^{3,31,32}, in that the similarity in the system's mass fraction to those of Jupiter and Saturn would then be causal rather than coincidental. Further work incorporating the origin of the uranian obliquity is needed to ultimately distinguish between these alternatives.

Although the model presented here applies to regular satellite formation, it is remarkable that Neptune's single large, irregular satellite, Triton, also contains a similar mass fraction, with $M_{\text{Triton}}/M_p \approx 2.1 \times 10^{-4}$. Triton's orbit is retrograde and inclined, and it is believed to have been captured intact from heliocentric

orbit^{33–35}. Although we lack direct evidence of a putative^{33,35,36} original prograde neptunian satellite system, it seems clear that it cannot have contained much greater total mass than Triton itself. Otherwise, a retrograde and initially eccentric Triton would have been destroyed while traversing the regular satellite region (either as it was accreted or collisionally disrupted, or by the decay of its orbital angular momentum³⁶ owing to interactions with a much greater mass in prograde material). The survival of a captured retrograde satellite requires it to have comparable or greater mass than any prograde system with which it actively interacts. As larger interlopers would have been less numerous (and therefore captured less frequently), the most probable surviving Triton-like object would be one having the smallest mass affording its survival, which would suggest that M_{Triton} is similar to the total mass of Neptune's original regular satellites, or $M_T/M_{\text{Neptune}} \approx O(10^{-4})$ as well.

General implications

When more than a few per cent of a gas planet's mass in solar composition material is processed through a circumplanetary disk, one or more generations of inflow-produced satellite systems are likely^{9,23}, with earlier satellites doomed to collision with the planet. Today's observed satellites are then the last generations that formed as inflow to the planets waned, implying that they formed very slowly in low-pressure, 'gas-starved'³⁷ disks. For extrasolar giant planets orbiting within their stellar habitable zone, the prospect has been raised of the existence of habitable environments on hypothesized Earth-sized satellites^{38,39}. Provided that such planets accumulated gas while contracted to scales consistent with circumplanetary disks (which appears likely for nebular removal timescales $\geq 10^6$ years^{8,40}; Supplementary Notes), the findings here imply that their largest surviving satellites would contain on the order of $10^{-4}M_p$, so that a Jupiter-mass exoplanet would host only Moon-to-Mars sized satellites.

Received 13 March; accepted 5 May 2006.

- Jewitt, D. & Sheppard, S. Irregular satellites in the context of planet formation. *Space Sci. Rev.* **116**, 441–455 (2005).
- Stevenson, D. J., Harris, A. W. & Lunine, J. I. in *Satellites* (eds Burns, J. A. & Matthews, M. S.) 39–88 (University of Arizona Press, Tucson, 1986).
- Pollack, J. B., Lunine, J. I. & Tittlemore, W. C. in *Uranus* (eds Bergstrahl, J. T., Miner, E. D. & Matthews, M. S.) 469–512 (University of Arizona Press, Tucson, 1991).
- Lunine, J. I., Coradini, A., Gautier, D., Owen, T. C. & Wuchterl, G. in *Jupiter: The Planet, Satellites and Magnetosphere* (eds Bagenal, F., Dowling, T. E. & McKinnon, W. B.) 19–34 (Cambridge University Press, Cambridge, UK, 2004).
- Calvet, N., Hartmann, L. & Strom, S. E. in *Protostars and Planets IV* (eds Mannings, V., Boss, A. P. & Russell, S. S.) 377–399 (University of Arizona Press, Tucson, 2000).
- Lubow, S. H., Seibert, M. & Artymowicz, P. Disk accretion onto high-mass planets. *Astrophys. J.* **526**, 1001–1012 (1999).
- Bate, M. R., Lubow, S. H., Ogilvie, G. I. & Miller, K. A. Three-dimensional calculations of high- and low-mass planets embedded in protoplanetary discs. *Mon. Not. R. Astron. Soc.* **341**, 213–229 (2003).
- Papaloizou, J. C. B. & Nelson, R. P. Models of accreting gas giant protoplanets in protostellar disks. *Astron. Astrophys.* **433**, 247–265 (2005).
- Canup, R. M. & Ward, W. R. Formation of the Galilean satellites: Conditions of accretion. *Astron. J.* **124**, 3404–3423 (2002).
- Ward, W. R. On disk-planet interactions and orbital eccentricities. *Icarus* **73**, 330–348 (1998).
- Artymowicz, P. Disk-satellite interaction via density waves and the eccentricity evolution of bodies embedded in disks. *Astrophys. J.* **419**, 166–180 (1993).
- Papaloizou, J. C. B. & Larwood, J. D. On the orbital evolution and growth of protoplanets embedded in a gaseous disc. *Mon. Not. R. Astron. Soc.* **315**, 823–833 (2000).
- Ward, W. R. Density waves in the solar nebula—Differential Lindblad torque. *Icarus* **67**, 164–180 (1986).
- Ward, W. R. Protoplanet migration by nebula tides. *Icarus* **126**, 261–281 (1997).
- Tanaka, H. & Ward, W. R. Three-dimensional interaction between a planet and an isothermal gaseous disk. II. Eccentricity waves and bending waves. *Astrophys. J.* **602**, 388–395 (2004).
- Tanaka, H., Takeuchi, T. & Ward, W. R. Three-dimensional interaction between a planet and an isothermal gaseous disk. I. Corotation and Lindblad torques and planet migration. *Astrophys. J.* **565**, 1257–1274 (2002).

17. Ward, W. R. Density waves in the solar nebula—Planetesimal velocities. *Icarus* **106**, 274–287 (1993).
18. Shakura, N. I. & Sunyaev, R. A. Black holes in binary systems. Observational appearance. *Astron. Astrophys.* **24**, 337–355 (1973).
19. Duncan, M. J., Levison, H. F. & Lee, M. H. A multiple timestep symplectic algorithm for integrating close encounters. *Astron. J.* **116**, 2067–2077 (1998).
20. Chambers, J. E., Wetherill, G. W. & Boss, A. P. The stability of multi-planet systems. *Icarus* **119**, 261–268 (1996).
21. Lissauer, J. J. Urey Prize Lecture: On the diversity of plausible planetary systems. *Icarus* **114**, 217–236 (1995).
22. Mosqueira, I. & Estrada, P. R. Formation of regular satellites of giant planets in an extended gaseous nebula I: Subnebula model and accretion of satellites. *Icarus* **163**, 198–231 (2003).
23. Alibert, Y., Mousis, O. & Benz, W. Modeling the Jovian subnebula. I. Thermodynamic conditions and migration of proto-satellites. *Astron. Astrophys.* **439**, 1205–1213 (2005).
24. Hubickyj, O., Bodenheimer, P. & Lissauer, J. J. Accretion of the gaseous envelope of Jupiter around a 5 to 10 Earth-mass core. *Icarus* **179**, 415–431 (2005).
25. Slattery, W. L., Benz, W. & Cameron, A. G. W. Giant impacts on a primitive Uranus. *Icarus* **99**, 167–174 (1992).
26. D'Angelo, G., Henning, T. & Kley, W. Thermodynamics of circumstellar disks with high-mass planets. *Astrophys. J.* **599**, 548–576 (2003).
27. Ward, W. R. & Hamilton, D. P. Tilting Saturn. I. Analytic model. *Astron. J.* **128**, 2501–2519 (2004).
28. Hamilton, D. P. & Ward, W. R. Tilting Saturn II. Numerical model. *Astron. J.* **128**, 2510–2517 (2004).
29. Goldreich, P. Inclination of satellite orbits about an oblate precessing planet. *Astron. J.* **70**, 5–9 (1965).
30. Brunini, A. Origin of the obliquities of the giant planets in mutual interactions in the early Solar System. *Nature* **440**, 1163–1165 (2006).
31. Canup, R. M. & Ward, W. R. A possible impact origin of the Uranian satellite system. *Bull. Am. Astron. Soc.* **32**, 1105 (2000).
32. Ward, W. R. & Canup, R. M. Viscous evolution of an impact generated disk around Uranus. *Bull. Am. Astron. Soc.* **35**, 1046 (2003).
33. Goldreich, P., Murray, N., Longaretti, P. Y. & Banfield, D. Neptune's story. *Science* **245**, 500–504 (1989).
34. McKinnon, W. B., Lunine, J. I. & Banfield, D. in *Neptune and Triton* (ed. Cruikshank, D. P.) 807–877 (University of Arizona Press, Tucson, 1995).
35. Agnor, C. B. & Hamilton, D. P. Neptune's capture of its moon Triton in a binary–planet gravitational encounter. *Nature* **441**, 192–194 (2006).
36. Cuk, M. & Gladman, B. J. Constraints on the orbital evolution of Triton. *Astrophys. J.* **626**, L113–L116 (2005).
37. Stevenson, D. J. Jupiter and its moons. *Science* **294**, 71–72 (2001).
38. Williams, D. M. & Kasting, J. F. Habitable moons around extrasolar giant planets. *Nature* **385**, 234–236 (1997).
39. Barnes, J. W. & O'Brien, D. P. Stability of satellites around close-in extrasolar giant planets. *Astrophys. J.* **575**, 1087–1093 (2002).
40. Burrows, A., Hubbard, W. B. & Lunine, J. K. The theory of brown dwarfs and extrasolar giant planets. *Rev. Mod. Phys.* **73**, 719–765 (2001).
41. Saumon, D. & Guillot, T. Shock compression of deuterium and the interiors of Jupiter and Saturn. *Astrophys. J.* **609**, 1170–1180 (2004).
42. Anderson, J. D. *et al.* Shape, mean radius, gravity field, and interior structure of Callisto. *Icarus* **153**, 157–161 (2001).
43. Johnson, T. V. & Lunine, J. I. Saturn's moon Phoebe as a captured body from the outer Solar System. *Nature* **435**, 69–71 (2005).
44. Cassen, P. & Moosman, A. On the formation of protostellar disks. *Icarus* **48**, 353–376 (1981).
45. Klahr, H. H. & Bodenheimer, P. Turbulence in accretion disks: vorticity generation and angular momentum transport via the global baroclinic instability. *Astrophys. J.* **582**, 869–892 (2003).
46. Goodman, J. & Rafikov, R. R. Planetary torques as the viscosity of protoplanetary disks. *Astrophys. J.* **552**, 793–802 (2001).
47. Lin, D. N. C. & Papaloizou, J. C. B. in *Protostars and Planets III* (eds Levy, E. H. & Lunine, J. I.) 749–835 (University of Arizona Press, Tucson, 1993).
48. Ward, W. R. & Hahn, J. in *Protostars and Planets IV* (eds Mannings, V., Boss, A. P. & Russell, S. S.) 1135–1155 (University of Arizona Press, Tucson, 2000).

Supplementary Information is linked to the online version of the paper at www.nature.com/nature.

Acknowledgements This research was supported by NASA's Planetary Geology and Geophysics and Outer Planets Research programmes. Computer resources and support were provided by SwRI. We thank L. Dones, R. Mhiran and S. Peale for comments.

Author Information Reprints and permissions information is available at npg.nature.com/reprintsandpermissions. The authors declare no competing financial interests. Correspondence and requests for materials should be addressed to R.M.C. (robin@boulder.swri.edu).